FATIGUE LIFE AND FAILURE OF IMPACT-DAMAGED CARBON FIBRE COMPOSITES UNDER COMPRESSIVE CYCLIC LOADS

Fan Xu, Wenli Liu* and Phil E. Irving

Centre of Aeronautics, Cranfield University, Cranfield MK43 0AL, UK
*Corresponding author (wenli.liu@cranfield.ac.uk)

Keywords: Composites, Post impact fatigue, Damage tolerance

ABSTRACT

This paper explores and identifies delamination growth and failure processes in impact-damaged carbon fibre epoxy composites under compressive cyclic loading. Low velocity drop weight impacts were used to create the initial damage. There were four levels from 12J-25J. Maximum compressive loads during fatigue were between 70% and 80% of the nominal residual strength in compression after impact (CAI) tests. Delamination propagation was monitored at intervals during the test using DIC and C-scan techniques. It was found that compressive fatigue failure can be categorised into three phases: (1) local bending at impact damage site (2) local buckling mode change and (3) buckling propagation. Monitoring of local normal displacement at the impact damage site provided earlier indications of fatigue induced changes in delamination buckling than observations of delamination area growth. A three-dimension analytical model was developed and revealed that deep delamination has higher strain energy release rates at crack tip than delaminate at the surface of laminate.

1 INTRODUCTION

Approaches to damage tolerance certification in carbon fibre polymer composite aircraft structures are radically different from the equivalent in metallic aircraft. Demonstration of damage tolerance in aluminium aircraft is ensured via slow fatigue crack growth coupled with regular inspections so as to have a high probability of detection of fatigue cracks prior to any catastrophic event. In contrast damage tolerance in polymer composite aircraft structures requires demonstration of zero delamination growth, as once propagation starts, crack growth can be so fast there is no practical window for inspection to detect growing cracks. An important category of defects from which delamination can propagate is the local arrays of delamination formed subsurface after impacts to the structure.

Under compression- compression in-plane fatigue these delamination can grow under local mode I / mode II displacements once a threshold stress of around 70% of the static compression strength is exceeded. Despite a few previous investigations [1-6], factors controlling the onset of delamination growth and the stress and life at which growth begins are poorly understood.

Gerharz et al. [1] suggested two phases during the fatigue failure. The first stage was occupied by small buckling deformation and compliance increase. There was no delamination growth observed out of the damage envelope. The second stage, occupying the last 10% of the fatigue life exhibits rapid damage growth to failure. Research done by Beheshty and Harris [2] showed that for fatigue loading at R=10 no damage growth was detected until rupture was approached. Specimens loaded at R= -0.3 showed damage propagation in the direction of 45° plies. Ogasawara [3] et al. proposed a statistical model based on Weilbull distribution, and reported the ratio between the endurance limit at 10^6 and 10^7 cycles and the initial static strength was estimated at 0.74 and 0.68. Irving et al. [4] compared many reports on fatigue delamination growth and found inconsistency in the data reported. Some investigations reported zero delamination growth until just before failure and others found that delamination propagation occurs throughout life. Mitrovich et al. [5] in their investigation of fatigue delamination growth in composite materials observed that delamination propagation occurs much earlier in life and grows further. According to Garnier et al. [6], at the beginning of the Tension-Compression

fatigue test at 0.3 Hz, the defect evolves in the two directions of the loading plane. After stabilisation the defect propagation appears only along the direction perpendicular to the load direction. The reasons for it was not explained. Melin et al. [7] conducted experiments in constant amplitude tension–compression fatigue and monitored the process using an optical whole field measurement technique. Delamination propagation and local buckling was found only during compression period.

This paper will explore and identify the delamination growth and failure process in impact-damaged carbon fibre epoxy composites under compressive cyclic loading and analyse the experimental observations using linear elastic fracture mechanics and numerical modelling.

2 EXPERIMENTAL TESTS

2.1 Specimen

The material of this study is HexPly AS7/8552 prepreg tape from Hexcel with a ply thickness of 0.135mm. The samples were stacked using a 32 ply quasi-isotropic layup ($[45/0/-45/90]_{4s}$). The specimen was cut from a 600 mm square panel with individual specimen size of 150 mm × 100 mm in accordance with the testing standard ASTM D7136 [9]. The cured sample had an average thickness of 4.4 mm. The lamina properties of the material are shown in Table 1 [10].

Table 1 Lamina properties of UD AS7/8552 prepreg

Properties	Value	
Longitudinal Modulus E_1	145	GPa
Transverse Modulus E_2	10	GPa
Poisson's Ratio v_{12}	0.3	
Shear Strength G_{12}	5.8	GPa
Ply Thickness t_{ply}	0.135	mm
Longitudinal Tensile Strength 0°	2550	MPa
Transverse Tensile Strength 90°	90	MPa
Longitudinal Compression Strength 0°	1862	MPa
Transverse Compression Strength	180	MPa
In Plane Shear Strength	115	MPa

2.2 Low velocity impact and compression after impact measurement

Low velocity impact testing was conducted to introduce impact damage in the specimens. Impact testing was carried out within the framework of ASTM 7136. The test standard requires use of a 16mm diameter impactor and a fully clamped support with an inner window size of 75 mm × 50 mm. Impact testing was performed using a Rosand Instrumented Falling Weight machine. Four energy levels (12J, 15J, 20J, 25J) were used producing different extents of delamination damage. The impactor was maintained at the same weight; different energies being achieved by altering the impactor height. The dent depths caused by the impact were measured by a coordinate measuring machine (CMM) after the impact. All the depths were categorised in the BVID range (< 0.5 mm).

Eight impacted specimens (two for each energy level) had their residual compressive strength under quasi-static compression load measured (constant displacement rate of 0.05mm/s). Tests were performed using a static 600 kN hydraulic machine. All the tests were in compliance with ASTM 7137 [11] for CAI testing. An anti-buckling guide was used in the tests. The guide had clamped edge restraints and simply supported restraints for the test object in x-direction and y-direction in the laminate local coordinate system. The anti-buckling guide ensured that proper displacement was maintained in longitudinal direction (loading direction) and enough space for the sample to break in transverse direction.

2.3 Fatigue testing

Fatigue testing was performed using a 250 kN servo-hydraulic system. There is no currently agreed or published testing standard for post impact fatigue testing; the static CAI jig was adapted for use in the subsequent cyclic period. Before fatigue testing, samples were impacted at the same energy levels as used previously and then subjected to in-plane compression-compression fatigue loading. The ratio between the maximum compressive stress and the initial static CAI strength was between 0.7 and 0.8. Test frequency was limited to 5Hz to avoid thermal heating and R ratio was 10 for all fatigue tests. The test was interrupted at intervals for ultrasonic and digital correlation image measurements. The setting of the experimental tests is shown in Figure 1.

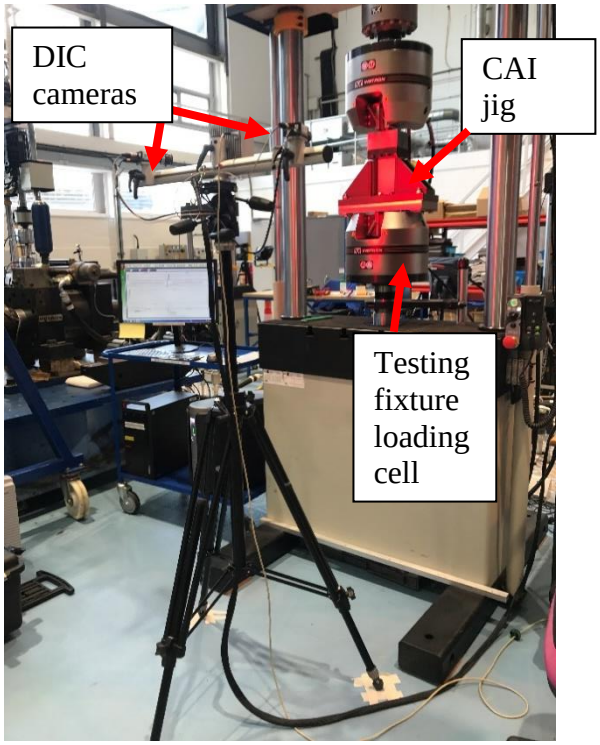

Figure 1: Specimen, fixture, testing rig and DIC equipment used for fatigue testing.

2.4 Non-Destructive monitoring of damage growth during fatigue

Ultrasound C-scan was used to monitor delamination area and Digital Image Correlation (DIC) monitored surface strain and displacements in three directions throughout the test. Ultrasound monitoring used a multiphase ultrasonic system. The 5MHz probe consists of 64 groups of transducers to inspect the sample in various ways. The DIC system was adapted during the fatigue after impact (FAI) tests to acquire normal displacement and surface strain changes at intervals throughout the test. The capture rate was 100ms and the loading rate was altered to 1Hz while image data was being recorded to maximise the number of pictures taken during a loading cycle. Tests were stopped at 5×10^5 cycles and samples regarded as a run-out. The stiffness K of a sample at certain cycle under fatigue loading was defined the ratio of load range ΔF to displacement range ΔD within a loading half cycle, which is expressed by

$$K = \frac{\Delta F}{\Delta D} \tag{1}$$

where $\Delta D = D_{\max} - D_{\min}$ and $\Delta F = F_{\max} - F_{\min}$, and $F_{\max}$ is maximum load and $F_{\min}$ is minimum load in a half fatigue cycle. $D_{\max}$ and $D_{\min}$ are the corresponding maximum and minimum displacements, respectively. The $D_{\max}$ and $D_{\min}$ are calculated from the difference of values from two 80 mm gauges marked at top and bottom edge from the DIC capture. A

schematic drawing for the stiffness calculation during a fatigue cycle is presented in the following figure.

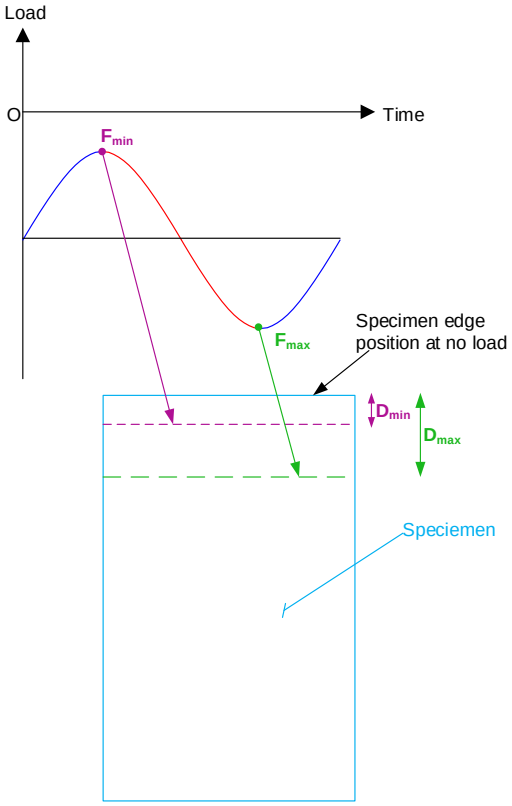

Figure 2: Schematic drawing of global stiffness calculation during a fatigue cycle.

3 ANALYTICAL MODELLING

For interpretation of testing observation and further prediction of fatigue life limit, strain energy release rates (SERR) were calculated according to concept of linear elastic fracture mechanics. Typically, delamination growth is assumed to be governed by SERR of G_I, G_{II} and G_{III} for the three fracture modes, respectively. Virtual crack closure technique (VCCT) was used to obtain three SERRs on the delamination tips, which assuming that the energy required to open a crack is equal to the one to close the crack. VCCT was implemented using the commercial FE package ABAQUS.

A complete three-dimension FE model was developed using continuum shell elements with 8 nodes, i.e. SC8, which is particularly provided by ABAQUS to model multiple delamination throughout laminate thickness. Circular shapes of delamination with 40 mm diameter were inserted between ply interfaces to simulate initial impact damage based on the maximum delamination area obtained from C-scan. Compressive load and boundary conditions were set exactly the same as the experimental tests, which will show in details together with results in Section 4.3.

4 RESULTS AND DISCUSSION

4.1 Fatigue Life

Table 2 shows the initial damage area, the maximum compressive stress and the fatigue life obtained for all the test samples. Samples with different damage areas were tested at a range of different stresses to maintain the ratio of fatigue stress to CAI stress the same. In general it was found that samples with small impact damage area had greater fatigue strength and longer lives than samples with large damage area despite being tested at the same ratio of fatigue to static strength.

Table 2 Experimental results of fatigue after impact tests

Sample ID	Initial Damage Area (mm^2)	Nominal CAI Percentage	Max. Compressive Stress (MPa)	Total Cycles
Q12-7	756.9	85%	217.1	146785
Q12-3	809.8	80%	204.4	>500000
Q12-4	889.9	82%	209.5	>500000
Q15-3	1132.2	80%	196.3	1706
Q15-4	1023.0	77%	188.9	274815
Q15-5	939.3	75%	184.0	61865
Q15-8	1021.2	73%	179.2	> 500000
Q15-9	1079.5	70%	171.8	> 500000
Q20-2	1453.3	80%	170.6	6142
Q20-3	1416.7	77%	164.1	16497
Q20-4	1515.3	75%	160.0	31814
Q20-5	1484.4	73%	155.8	11300
Q20-7	1437.9	70%	149.3	>500000
Q25-1	1543.8	80%	154.9	1906
Q25-2	1597.5	77%	149.1	6501
Q25-3	1504.2	75%	145.1	8966
Q25-4	1552.0	73%	141.2	45465
Q25-6	1497.2	70%	129.2	> 500000

Figure 3 shows the fatigue lifetime of samples plotted against impact damage area for selected values of the ratio of fatigue stress to CAI. The fatigue life decreases with increasing damage area, even though the samples were tested with the maximum compression stress at the same fraction of static CAI strength. In addition for a given damage size, the larger the stress ratio, the smaller the life. For example the smallest lives are found for tests of $\sigma_{max}/\sigma_{CAI} = 0.8$, and the longest lives at $\sigma_{max}/\sigma_{CAI} = 0.73$. All samples tested at $\sigma_{max}/\sigma_{CAI} = 0.70$ ran out without failure.

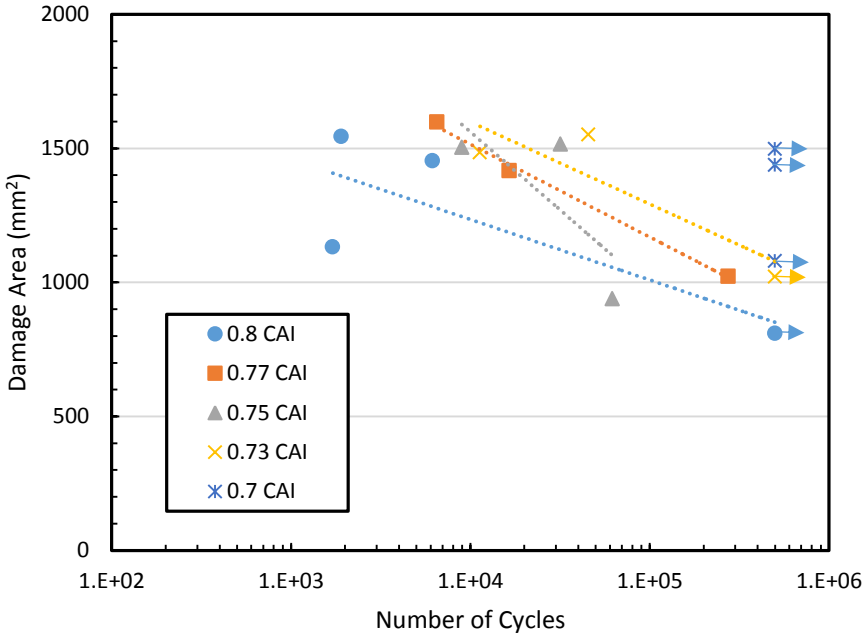

Figure 3: Fatigue life plotted against damage area of samples tested under same percentage of nominal CAI.

4.2 Delamination growth under fatigue

Evolution of compressive buckling at the damage site during fatigue testing was monitored via DIC measurements of normal displacement. All the samples which eventually failed had similar characteristics during fatigue cycling. The run-out samples remained unchanged no matter which observation method was used. Figure 4 shows three stages of failure progression of sample Q25-2 which failed after 6501 cycles at 0.77 CAI with a 25 J impact. At the beginning of fatigue life (1 cycle), delamination buckling had one half-wavelength bending inward with a displacement of -0.6 mm. The dent area was severely deformed. As cycle number increases to 5000, the delamination buckling mode changed to two half-wavelengths, one positive, and one negative. Between cycle 1 to cycle 5000, it can be found no obvious change at the checkpoint (N=2000) and gradual extrusion of the positive wavelength from N=3000. At this stage it is worthwhile noticing that there is no delamination propagation detected by the C-scan image at 5000 cycles. During the third stage at 6150 cycles, the local buckling propagated to one side of the edge along with in the C scan images, the propagation of detectable delamination.

Normal displacement data was extracted from DIC data on the midline of the sample surface and is plotted as a function of longitudinal position in Figure 5. At the beginning of fatigue, the impact damage area underwent a simple bending displacement inward as the displacement value is all negative. As the cycle number increased, the top surface of damage area generated the local buckling outwards the panel. As more fatigue cycles were added, the two half wavelength buckling extended to the edge and resulted in the fatal failure.

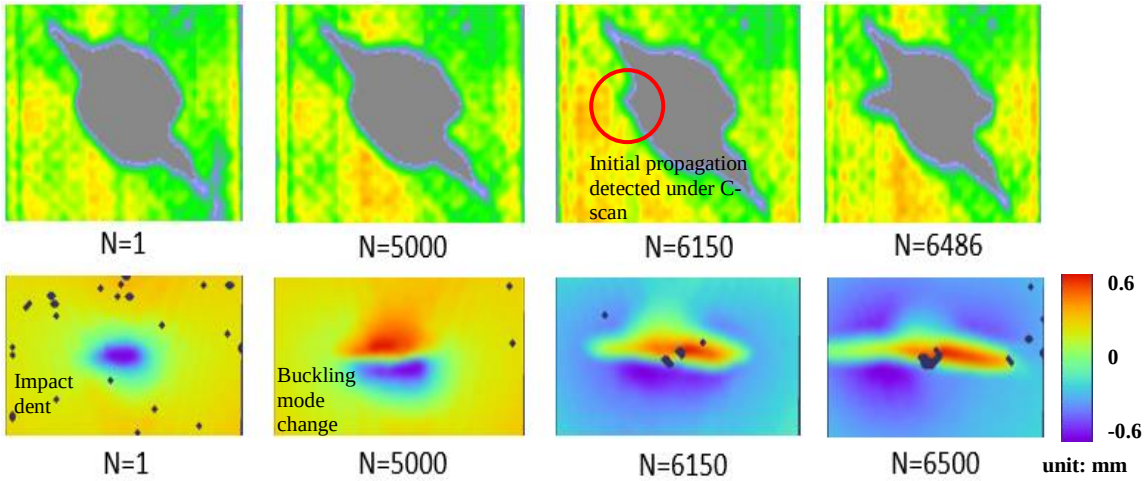

Figure 4: upper row: Delamination area detected from c-scan at 1, 5000, 6150, 6486 cycle(s); lower row: Out-of-plane displacement of sample Q25-2 from DIC measurement at 1, 5000, 6150 and 6500 cycle(s).

Another phenomenon worth stating as the initial delamination size is around 44 mm in longitudinal direction (see Figure 6), the pre-rupture cycles illustrates the 'envelope' of the same size even though the buckling mode has changed. The buckling mode only changes a few cycles before failure. The sudden increase in the delamination in the transverse direction leads to the ultimate failure.

.

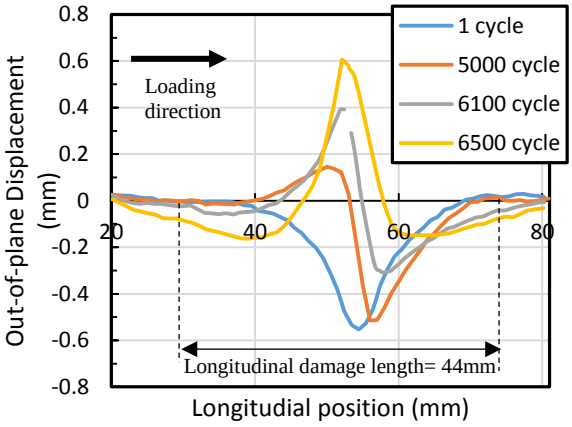

Figure 5: Out-of-plane displacement of sample Q25-2 on midline along the loading direction (section selected of a ±25 mm range).

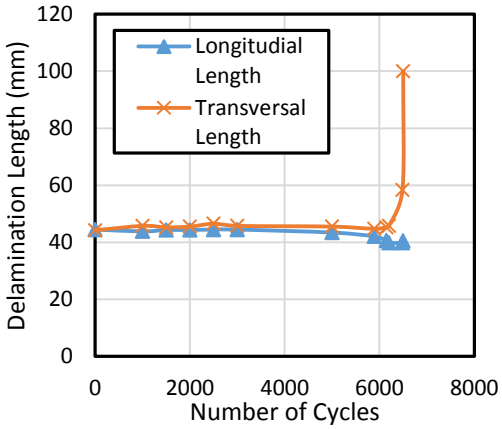

Figure 6: Longitudinal and transverse delamination length of sample Q25-2.

Observation of global stiffness (see figure 7) shows detectable reduction at 5000 cycles (76.9% of the fatigue lifetime) whereas the C-scan image showed delamination growth at 6150 cycle (94.6% of the fatigue lifetime). The degradation in global stiffness implies delamination propagation in the sample. Combining this observation with the late detection using C-scan of delamination projected area growth, it can be deduced that when impacted composites are under cyclic loading, the delamination propagation first occurs at the interfaces with smaller delaminations located deeper within the laminate. When delaminations in those interfaces propagate to a similar size of the overall projected damage area, the delamination grow to enlarge the previous envelope boundary. When most of the delaminations grow to the initial overall size, the composite panel becomes too vulnerable to sustain the previous load thus cause the fatal failure after little cycle increment.

The results from DIC and C scan are compared in Figure 8 in terms of the fraction of fatigue life at which damage growth was first detected for each technique. The ratio of the number of cycles to the initial observed buckling mode change to the fatigue life (R_d) using DIC measurement and the ratio and the ratio of initial delamination area propagation detection under to the fatigue lifetime (R_c) under C-scan for each test sample is plotted. A data point located above the dotted line means the DIC detected change appeared before C-scan detection while the points on the line imply simultaneous detection. These observations reveal not only the fatigue progress at a much earlier stage than previously reported but also that DIC can detect the progression much earlier than ultrasonic C-scan.

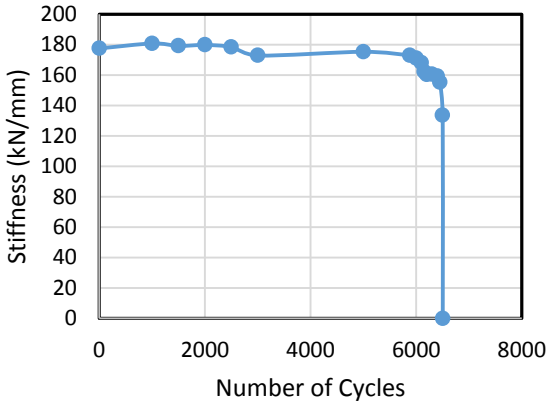

Figure 7: Global stiffness reduction of sample Q25-2.

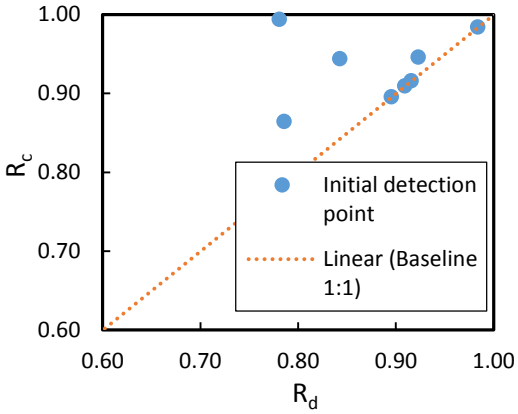

Figure 8: Comparison of the R_c and R_d.

The observation of changes in delamination buckling shape and stiffness degradation obtained by DIC suggest delamination in deeper interfaces from the backside grows at an earlier stage of fatigue than is visible via C-scan.

4.3 SERR from analytical modelling

The layup in the FE model has 32 plies and the stacking sequence is kept the same as the experimental coupons. The relevant material properties are shown in Table 1 and the critical SERRs of G_{IC} and G_{IIC} are 241 and 840 J/m^2, respectively [14]. The mesh size is controlled as small as 1 mm around the delamination tip and eventually becomes large size of 5 mm in the region away from crack tips for compromising computation time and accuracy, as shown in Fig. 9. A total number of 71866 elements were used.

Figure 9 illustrates a typical delamination buckling mode of half-wavelength containing a circular delamination, which can be inserted in each ply interface through laminate thickness. It was found that the model having a delamination between the first and second plies gave the lowest delamination buckling load which is obviously due to the lowest stiffness of its surface sub-laminate. This local buckling mode obtained from the linear eigenvalue analysis was then transferred to a following non-linear static analysis by less than 0.1% imperfection to guide this fracture FE model through a correct bifurcation point.

Furthermore, in the FE model for fracture analysis, a second delamination was inserted between the fifth and sixth plies and SERRs at two delaminations were calculated by VCCT. Although the thin sub-laminate with the delamination at the first ply interface was buckled first, the G_I and G_{II} at its delamination tip are only 20% and 0.5% of the thick sub-laminate with the delamination at the fifth ply interface. This result could explain that during fatigue tests, the deep impact damage grew first because similarly, under cyclic loading, the range of ΔG would be higher in the deep delamination surface. Hence the crack growth occurs earlier than the delamination toward the surface of laminate.

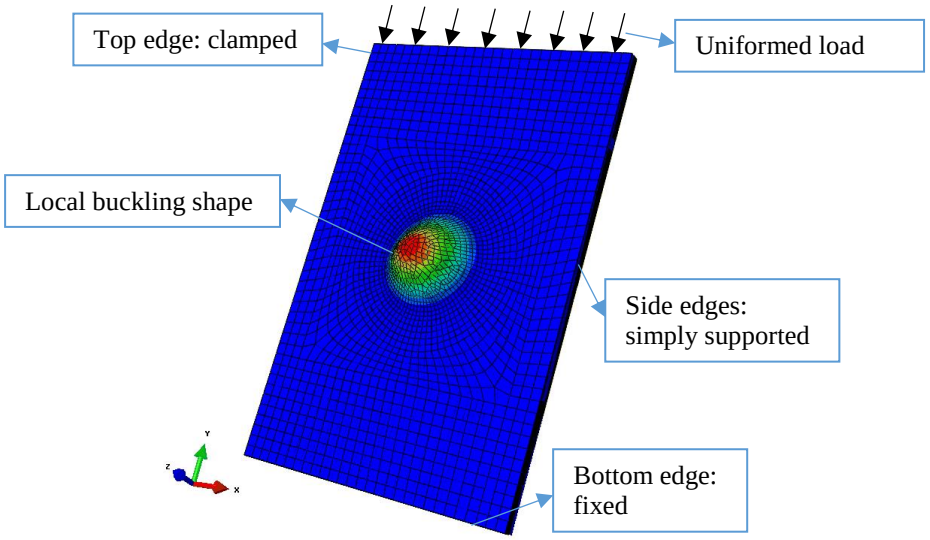

Figure 9: Illustration of boundary conditions and numerical model of local buckling with the delamination locates between 1st and 2nd plies.

5. CONCLUSIONS AND FUTURE WORK

Samples of impacted carbon fibre composites were tested in compressive fatigue to explore and identify the delamination growth and failure process. Stress level at the growth/non-growth transition for different levels of impact energy were recorded and the relationship between fatigue life and initial damage area is quantified. 70% nominal CAI stress is the stress level to ensure 5×10^5 lifetime, while for the less impact damage cases (12J) the stress level to ensure no failure can be lifted as high as 82%. All the samples undergoing eventual failure have similar failure progression. The run-out samples remain unchanged no matter which observation method was used. For the failed samples, compressive fatigue failure can be categorised into three stages: (1) local bending at impact damage site (2) local buckling mode change and (3) buckling propagation. Monitoring of local normal displacement at the impact damage site provids earlier indications of fatigue induced changes in delamination buckling than observations of delamination area growth. The latter could be detected only after 95% of the life had been consumed. Before delamination propagation could be detected by C-scan, there were changes in delamination buckling shape and stiffness degradation obtained by DIC measurements. This suggests delamination at deeper interface propagation at an early stage of fatigue. Numerical modelling results give some insights into why smaller and deeper delamination are prone to grow due to high strain energy release rates.

Although the behaviour of the rest of the testing samples was similar, the details are still being analysed for an inter-group comparison and cross-group comparison to investigate the out-of-plane displacement and Rc, Rd value related to impact energy, damage area and stress level. More modelling work will be accomplished for the maxtix of different location and size of the delaminations.

ACKNOWLEDGEMENTS

The authors wish to thank Mr. Barry Walker and Mr. Jim Hurley of Cranfield University for their help with fatigue experiments and sample curing.

REFERENCES

[1] J. J. Gerharz, H. Idelberger, H. Huth, Impact damage in fatigue loaded composite structures. *Proceedings of the 15th Symposium of the International Committee on Aeronautical Fatigue*, Israel, 1989, pp. 497–516.

[2] M. H. Beheshty, B. Harris, Post-impact fatigue behaviour of CFRP and the growth of low-velocity impact damage during fatigue. *Proceedings of the International Conference on Fatigue of Composites*, France, 1997, pp. 355–62.

[3] T. Ogasawara, S. Sugimoto, H. Katoh, and T. Ishikawa, Fatigue behavior and lifetime distribution of impact-damaged carbon fibre/toughened epoxy composites under compressive loading, *Advanced Composite Materials*, 22(2), 2013, pp. 65–78.

[4] G. Davies, and P. Irving, *Impact, post-impact strength and post-impact fatigue behaviour of polymer composites,* Polymer Composites in the Aerospace Industry, Chapter 9, Imperial College, London, United Kingdom: Elsevier Inc., 2014

[5] M. Mitrovic, H. T. Hahn, G. P. Carman, and P. Shyprykevich, Effect of loading parameters on the fatigue behavior of impact damaged composite laminates, *Composites Science and Technology*, 59(14), 1999, pp. 2059-2078.

[6] C. Garnier, M. Pastor, B. Lorrain and O. Pantalé, Fatigue behaviour of impacted composite structures, *Composite Structures*, 100, 2013, pp. 443-450.

[7] L. G. Melin and J. Schon, Buckling behaviour and delamination growth in impacted composite specimens under fatigue load: an experimental study, *Composites Science and Technology*, 61(13), 2001, pp. 1841–1852.

[8] R. Butler., A. T. Rhead, W. Liu and N. Knotis, Compressive strength of delaminated aerospace composites. *Philosophical Transactions of the Royal Society A: Mathematical, Physical and Engineering Sciences*, 370(1965), 2012, pp.1759–1779.

[9] ASTM D7136/D7136M-12. Standard test method for measuring the damage resistance of a fiber-reinforced polymer matrix composite to a drop-weight impact event. West Conshohocken (PA).

[10] Hexcel, "HexPly® 8552 Epoxy matrix (180°C/356°F) curing matrix," Product data sheet, 2016

[11] ASTM D7137/D7137M-12. Standard test method for compressive residual strength properties of damaged polymer matrix composite plates. West Conshohocken (PA).

[12] R. Krueger, Development of benchmark examples for quasi-static delamination propagation and fatigue growth predictions. *Proceeding of 27th Annual Technical Conference of the American Society for Composites 2012, Held Jointly with 15th Joint US-Japan Conference on Composite Materials and ASTM-D30 Meeting*, USA, 2012, pp.1–14.

[13] M. Benzeggagh and M. Kenane, Measurement of mixed-mode delamination fracture toughness of unidirectional glass/epoxy composites with mixed-mode bending apparatus, *Composites Science and Technology*. 56 (4), 1996, pp.439-449.

[14] Y. Chen, Mixed Mode Delamination static and Fatigue Crack Growth of Unidirectional CFRP Composite Laminates. Cranfield University: 2015 (MSc Thesis)